Analyzing Hole Spin Qubit Characteristics

Ana M. Ciocoiu
Department of Electrical and Computer Engineering,
University of British Columbia
(Dated: March 27, 2023)

In this project, important properties of hole spins in single and double quantum dots (QDs) are investigated. The dipole matrix elements, Rabi time, spin-flip and spin-conserving tunneling elements are calculated and their electric and magnetic field dependence is analyzed. It is found that hole spin-flip tunneling in group IV semiconductors is dependant on electric field, and invariant with magnetic field. This provides insight into the best ways that high fidelity spin-readout procedures can be implemented using QDs.

I. INTRODUCTION

Spin qubits in silicon are a promising platform on which to implement quantum devices: they possess very long coherence times, have the desired exchange statistics, and are industrially manufacturable [1]. These qubits are generally implemented using Si MOS or Si/SiGe heterostructures [2].
Recent breakthroughs in silicon electron spin qubits include high accuracy single-qubit gates [3] and small-scale algorithms [4]. However, electron spin qubits in silicon suffer from several challenges that limit their scalability. Qubits can only be manipulated magnetically [5], and the conduction band valleys introduce an unwanted orbital degree of freedom into the system [1].

Hole spin qubits have several advantages over electron spin qubits. They lack the sixfold degenerate minima —valleys— that cause imperfect spin state control in electron-based qubits. Holes also have strong spin-orbit interaction, allowing for spin state manipulation using electric-dipole spin resonance (EDSR) techniques. Electric fields are much easier to apply and control than magnetic fields, making this approach more scalable. Holes have also been shown to exhibit long coherence times [6]. This means that devices based on these qubits would be able to compute more complex problems more power-efficiently.

Of special interest are quantum dot (QD) hole spin qubits based on Ge. This group IV element has zero nuclear spin (there will be no decoherence due to hyperfine coupling) and a very large g-factor, enabling operation at low magnetic fields.

The combination of unique crystal properties found in group IV elements with the Rashba spin-orbit interaction (SOI) mechanism unique to spin 3/2 systems leads to the existence of optimal qubit operation points, called "sweet spots", where the effect of dephasing due to electric field fluctuations is negligible. Since the Rashba SOI can be controlled electrically, the sweet spot can be found and optimized for each qubit.

In this project, calculations are done to determine the properties of single and double QD hole spin qubits. For single QDs, the effect of the electric field on Zeeman splitting, dipole matrix elements and Rabi time is determined. For DQDs, an analytic model from [7] is used to determine the spin-flip and spin-preserving tunneling terms. Determining the behavior of these terms as a function of QD separation and applied magnetic field is instrumental to finding optimal operation points for the qubits.

A prototype DQD platform is shown below, on the left side of Fig. 1. A two-dimensional hole gas forms at the hetero-interface, allowing the QDs to be electrostatically defined.

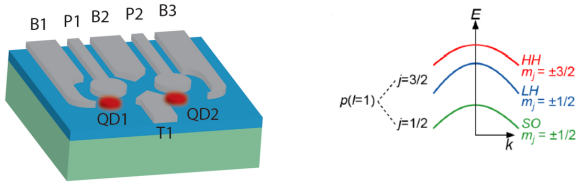

FIG. 1. Left: From [5]. A DQD platform composed of a thin strained Ge layer (green) grown between SiGe layers (not shown). A series of gates define the QDs (red). B2 and T1 control tunneling. Right: Diagram of the valence bands of interest in this study. The degeneracy between the HH and LH bands can be lifted due to compressive strain. From [8].

II. ANALYSIS OF SINGLE QD SYSTEM

A. Methods

To provide a background for benchmarking the DQD system, a single QD system is simulated. A thin, strained Ge layer is used as a substrate.
The valence band structure of Ge is illustrated in the right of Fig. 1. Atomic SOI will introduce spin splitting at zero magnetic field, leading to an energy difference in the valence bands with different total angular momenta. This leads to a splitting of the $J = 3/2$ band and the $J = 1/2$ split-off (SO) hole band. The $J = 3/2$ band is

composed of the heavy-hole (HH) band with $m_J = \pm 3/2$ and the light-hole (LH) band with $m_J = \pm 1/2$.
The HH states will be used as basis states for qubit operation.

Application of a magnetic field B will further split the states in these bands by the Zeeman energy, $E_{Zm} = \frac{g\mu_b B}{2}$, where g is the g-factor, and μ_b is the Bohr magneton. An applied electric field will modify the g term.

A confining harmonic potential $U(r)$ is applied within the x-y plane, leading to formation of a single QD near the surface. A perpendicular electric field, E_z is also applied. This field will be used to control the strength of the Rashba SOI term. The system's eigenstates are then solved for using an existing scripted Kohn-Luttinger (K-L) solver.
The K-L model [9] allows for representation of a wavefunction as a sum over valence band Bloch functions multiplied with slowly varying functions that depend on the applied potential $U(r)$:

$$\psi(r) = \sum_{J,m_J} F_{J,m_J}(r)\phi_{J,m_J}(r). \tag{1}$$

The solver considers the Bloch functions to be known and only solves for the $F_{J,m_J}(r)$ functions. The spinor basis for this Hamiltonian consists of only HH and LH states:

$$\left\{ |\frac{3}{2},\frac{3}{2}\rangle\, |\frac{3}{2},-32\rangle\, |\frac{3}{2},\frac{1}{2}\rangle\, |\frac{3}{2},\frac{-1}{2}\rangle \right\} \tag{2}$$

The Hamiltonian, written in this basis, is:

$$(H(k) + H_\epsilon + H_Z + U(r))F(r) = EF(r) \tag{3}$$

where $H(k)$ is the kinetic energy operator, H_ϵ is a Bir-Pikus Hamiltonian for strain, H_Z is the Zeeman Hamiltonian, and $U(r)$ is the applied potential.

The wavefunction solutions are obtained for the first 4 energy states, and then used to calculate the quantities of interest.

B. Results and Discussion

A 7nm thick layer of Ge is simulated within a square 30nm grid. The confining potential is set up to create a QD with a radius of 8nm. The perpendicular gate electric field E_z is swept from 1 to 30MV/m. The potential applied to the system $U(r)$ is:

$$U(r) = qE_z z + \frac{m\omega^2}{2}((x-x_0)^2 + (y-y_0)^2) \tag{4}$$

The obtained E_{Zm} as a function of this electric field is shown on the left side of Fig. 2.
Dipole matrix elements p_{ijk} represent the interaction of the wavefunction dipole moments with the applied electric field; the indices i, j are placeholders for the index of the energy eigenvalue solutions.

$$p_{ijk} = \int \psi_i(r)^* q x_k \psi_j(r) d^3r \tag{5}$$

Elements with $i \neq j$ represent energy level transitions driven by a field applied along the $x = k$ direction in space, and elements where $i = j$ represent a lowest order correction term to a perturbation of the electric field along the k direction.

The dipole matrix elements of interest are p_{12x} and $p_{22z} - p_{11z}$ The magnitude of the former determines the speed of Rabi oscillations from the ground to excited state, while the latter will allow us to determine the effect of electric field noise on the qubit's dephasing rate. These terms are calculated and shown on the right side of Fig. 2.

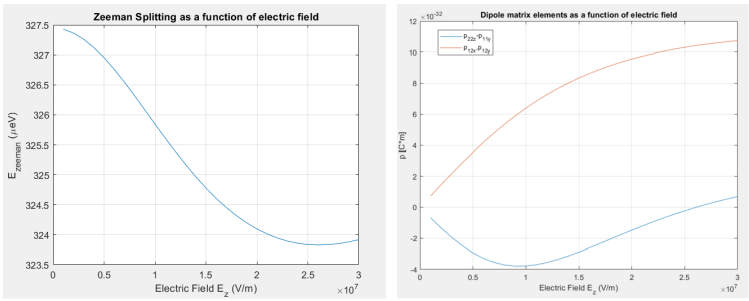

FIG. 2. Left: E_{Zm} as a function of E_z. A sweet spot is obvious around 26MV/m. Right: Dipole matrix elements p_{12x} (identical to p_{12y} due to symmetry) and $p_{22z} - p_{11z}$ as a function of E_z.

At the sweet spot, the value of p_{12x} is $1.1x10^{-31}[Cm]$. This term increases with the electric field, and seems to tend towards a peak value just past the sweet spot. The Rabi time is found to be proportional to $\frac{1}{p_{12x}}$ and is calculated to be 40ns in this case.
The $p_{22z} - p_{11z}$ element is zero at the sweet spot. This means that any electric field noise will not affect the existing splitting between the ground and excited energy levels; there will be no dephasing when operating the qubit at this sweet spot.

III. ANALYSIS OF DQD SYSTEM

A. Methods

Hole spins in DQDs are rich in phenomena absent from the single QD system just studied. Harnessing the properties of DQD systems means that more complex two-qubit gates can be created; additionally, spin initialization and readout schemes become feasible. Together, this builds the backbone of a practical spin qubit architecture. The starting Hamiltonian for hole spins in a DQD is taken from [7]:

$$H = -\frac{\epsilon}{2}\tau_z - t_c\tau_x + \frac{g}{2}\mu_B B\sigma_z + \eta\tau_y\sigma_y + \chi\tau_z\sigma_x \tag{6}$$

where χ and η are intra and inter dot spin flip tunneling respectively, t_c is spin-conserving tunneling coupling,

and ϵ is the detuning. The σ and τ terms are Pauli and position operators. The paper [7] uses perturbation theory to find an approximate form for the basis states; however, a more accurate basis consisting of the exact K-L eigenfunctions is used in this project. The first two single QD solutions are shifted to create either the left (QD1) or right (QD2) wavefunction solution of the system. These states, denoted $\psi_{l,\sigma}$ and $\psi_{r,\sigma}$ are then used to create orthogonal Wannier states:

$$|\psi_{L/R,\sigma}\rangle = \frac{|\psi_{l/r,\sigma}\rangle - \gamma\,|\psi_{r/l,\sigma}\rangle}{\sqrt{1-\gamma S-\gamma^* S^* + |\gamma|^2}} \tag{7}$$

where S represents the inner product of $\langle\psi_{l,\sigma}|\psi_{r,\sigma}\rangle$ and γ is $1-\sqrt{1-S^2}$. Note that the $\psi_{L/R,\sigma}$ Wannier states each contain a weighed sum of the real left and right QD wavefunction solutions.
This new basis for the Hamiltonian in (6) is written as:

$$\{|L,\uparrow\rangle, |L,\downarrow\rangle, |R,\uparrow\rangle, |R,\downarrow\rangle\} \tag{8}$$

The approach for calculating the spin tunneling terms is simplified somewhat by the fact that the Hamiltonian in (6) has been partially solved for by the K-L solver in the single QD case. Therefore, (6) can be rewritten as

$$H = H_0 + H' = K + U_L + U_R + H'. \tag{9}$$

Since K is simply the K-L Hamiltonian, and $U_{L/R}$ the harmonic potential defined in (4) centered around the new QD centers, a simple solution can be found for H'.

By rewriting (6) in matrix form, simple expressions for the expectation value of H were derived to yield the numerical value of the χ, η, and t_c terms. The behavior of these terms as a function of QD separation, applied B field, and E_z value is calculated and analyzed in the next section.

B. Results

The QDs each have a radius of 8nm, and both lie within a grid that is only 30nm wide. It is therefore important to provide sufficient separation distance, r_{sep}, between them for the calculation of the matrix elements. Since the left and right wavefunctions are created by shifting the single QD solution, there will likely be a limit on the possible values of r_{sep}. An upper bound on the allowable separation distance is determined by finding the 1-D dot product (along x, the direction in which the single wavefunction was shifted to create two separate QDs) of $\psi_{l,\sigma}$ with $\psi_{r,\sigma}$ and ensuring its maximum is larger than the minimum value of the single QD wavefunction over all its m_j states.
A maximum separation distance of 26nm is found. This is shown on the left side of Fig. 3.
A minimum bound on r_{sep} is found by comparing the Zeeman splitting value found by the K-L solver to the difference between the calculated on-diagonal matrix elements (which should also give the Zeeman energy). Convergence of this solution is observed for separation distances larger than 15nm. The remaining difference between the real and calculated E_{Zm} values is attributed to numerical error. This is shown on the right side of Fig. 3.

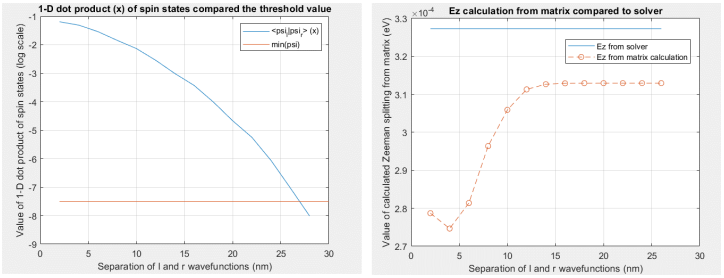

FIG. 3. Left: Finding an upper bound for the separation distance. Right: Finding a lower bound for the separation distance.

The matrix elements are calculated for B=0.1T, and $E_z = 3MV/m$ and plotted on the left as a function of r_{sep} in Fig. 4. On the right, the ratio of η to t_c is plotted.

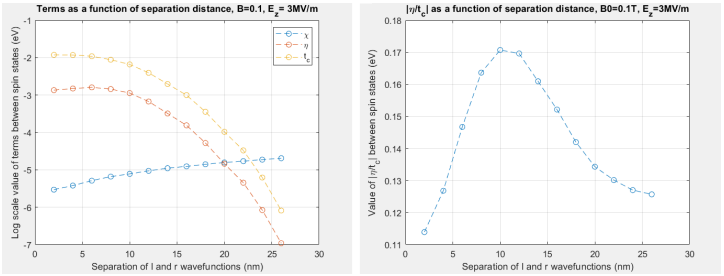

FIG. 4. Matrix elements of interest (left). Ratio of η to t_c (right).

As expected, the η and t_c terms decrease as a function of r_{sep}. This is a good check that the calculations obey the laws of physics. It is unclear why χ increases. The ratio of η to t_c will define the fidelity of the spin readout procedure.

Spin readout in spin QD systems is accomplished by spin-selective tunneling from one dot into the other. In the case of a DQD, tunneling of the electrons into the same dot is allowed only in the case of a spin singlet state (due to the Pauli exclusion principle)[10]. If the spin-flip tunneling is appreciably large, this readout mechanism becomes unreliable. The behavior of the spin flip tunneling term as a function of changes in magnetic and electric field strengths is further investigated.

For the former, a mid-range separation distance $r_{sep} = 20nm$ and field $E_z = 3MV/m$ is chosen for all calculations. The matrix elements are then calculated for a

magnetic field sweep from 0.01 to 0.3T. These results are shown on the left side of Fig. 5.

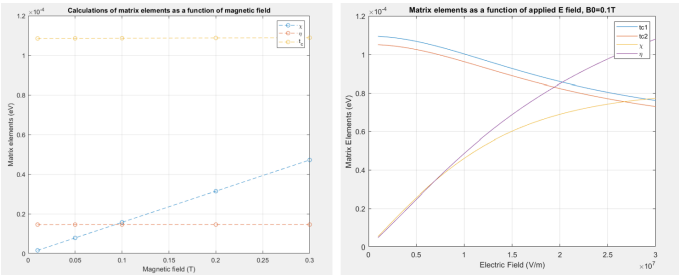

FIG. 5. Left: Matrix elements χ, η, and t_c as a function of B field. Right: Same elements as a function of E_z field, at 0.1T. Numerical error causes a small difference in half of the calculated t_c terms; ideally these should be equal.

The behavior of χ, η, and t_c matches the observed behavior in [7]: only χ increases linearly with magnetic field, and falls to a value of zero when the field is turned off.

This means that readout error due to spin flips *within* a single QD can be slightly improved by reducing the magnetic field strength during the procedure. However, the ratio of η to t_c stays constant over the entire range of magnetic field values studied: overall, this means that significant readout error will still exist. It has been previously theorized that the existence of singlet-triplet relaxation at low B field may be due to a variety of complex phonon interactions [10]. Spin-lattice (T1) and spin-spin (T2) relaxation times, as well as dephasing time (T2*) will decrease due to relaxation processes, and are significant sources of decoherence [10]. The results from Fig. 5 (left) suggest that this relaxation may also be related to the magnetic-field invariant nature of the spin-flip tunneling term. Further investigation would be required to confirm.

Next, the behavior of the matrix elements as a function of electric field is simulated. For the same r_{sep}, and a 0.1T field, E_z is swept from 1 to 30 MV/m. These results are shown on the right side of Fig. 5.

The spin-flip tunneling, which depends on the Rashba SOI, will go to zero as E_z approaches zero. This is related to the unique properties of group IV materials: their inversion symmetry eliminates the Dresselhaus SOI, which persists at zero E_z [11].

Unlike the Dresselhaus SOI (and most electron spin systems) the Rashba SOI evolves non-linearly as a function of E_z [11], allowing spin-flip tunneling to go to zero at zero E_z. Therefore, to increase the fidelity of hole spin-readout, the electric field should be turned off entirely: the ratio of η to t_c should be zero at this point. It is much easier to suddenly turn off an electric field than it is to do so with a magnetic field, so this result would lend itself well to practical implementation.

IV. CONCLUSION

In this project, a single QD is first analyzed to determine an ideal operating point. At this 'sweet spot,' the qubit is immune to electric field noise, and will not experience any dephasing. The sweet spot can be reached because the Rashba SOI is tunable by varying the applied E_z. This is a unique property of hole spins in group IV semiconductors. The tunneling properties of spins in DQDs are also analyzed. It is found that spin-flip tunneling η, which is responsible for decoherence, is invariant with magnetic field but can be reduced by reducing the applied electric field. Therefore, a high-fidelity spin readout procedure for hole spins in DQDs can be achieved by rapidly turning off the electric field at readout. The magnetic field invariant behavior of η may explain why singlet-triplet relaxation persists at low magnetic field: however, further investigation is necessary.

REFERENCES

[1] M. Veldhorst, H. G. J. Eenink, C. H. Yang, and A. S. Dzurak, Silicon CMOS architecture for a spin-based quantum computer, Nature Communications **8** (2018).

[2] T. D. Ladd and M. S. Carroll, Silicon Qubits, Encyclopedia of Modern Optics (2018).

[3] J. Yoneda *et al.*, A quantum-dot spin qubit with coherence limited by charge noise and fidelity higher than 99.9, Nature Nanotech. **13** (2018).

[4] T. F. Watson *et al.*, A programmable two-qubit quantum processor in silicon, Nature (London) **555** (2018).

[5] Z. Wang *et al.*, Suppressing charge-noise sensitivity in high-speed ge hole spin-orbit qubits, Meso. and Nano. Physics (2019).

[6] T. Kobayashi *et al.*, Engineering long spin coherence times of spin-orbit systems, Nature Materials **20** (2021).

[7] P. M. Mutter and G. Burkard, Natural heavy-hole flopping mode qubit in germanium, Phys. Rev. Res. **3** (2021).

[8] R. Moriya *et al.*, Cubic rashba spin-orbit interaction of a two-dimensional hole gas in a strained-ge quantum well, Phys. Rev. Lett. **113** (2014).

[9] J. M. Luttinger and W. Kohn, Motion of electrons and holes in perturbed periodic fields, Physical Rev. **97** (1955).

[10] C. H. Yang *et al.*, Operation of a silicon quantum processor unit cell above one kelvin, Nature (London) **580** (2020).

[11] W. Zhanning *et al.*, Optimal operation points for ultrafast, highly coherent ge hole spin-orbit qubits, NPJ Quantum Inf. **7** (2021).